Check for updates

ADVANCED OPTICAL MATERIALS
www.advopticalmat.de

Nonlinear Dielectric Epsilon Near-Zero Hybrid Nanogap Antennas

Romain Tirole, Benjamin Tilmann, Leonardo de S. Menezes, Stefano Vezzoli, Riccardo Sapienza, and Stefan A. Maier**

High-index Mie-resonant dielectric nanostructures provide a new framework to manipulate light at the nanoscale. In particular their local field confinement together with their inherently low losses at frequencies below their bandgap energy allows to efficiently boost and control linear and nonlinear optical processes. Here, nanoantennas composed of a thin indium-tin oxide (ITO) layer in the center of a dielectric gallium phosphide (GaP) nanodisc are investigated. While the linear response is similar to that of a pure GaP nanodisc, it is shown that second harmonic generation is enhanced across a broadband wavelength range. On the other hand, third harmonic generation is only marginally enhanced around the epsilon-near-zero wavelength of ITO. Linear and nonlinear finite-difference time-domain simulations show that despite the high refractive index contrast leading to strong field confinement inside the antenna's ITO layer, the nanogap enhancement effect is mitigated by the low nonlinear volume of the nanogap layer and the antenna's behavior at the harmonic wavelength. Measurement of ITO and GaP nonlinear susceptibilities additionally show a comparative advantage for harmonic generation in GaP. These investigations deliver insights on the mechanisms at play in nonlinear nanogap antennas and their potential applications as nanoscale devices.

1. Introduction

The implementation of nonlinear optics at the nanoscale and at visible to near-infrared (near-IR) wavelengths is of great interest for technical applications such as quantum light sources, optical circuits and frequency control or biophotonics. Although nanoantennas provide a gateway to efficiently couple incident light into structures at the nanoscale, other aspects such as small interaction volume or low damage threshold remain challenging. In particular, the latter limits the possible usage of plasmonic structures made of (noble) metals, together with their significant Ohmic losses. Hence, all-dielectric materials have proven to be a promising alternative platform for nanophotonics. Of particular interest are group IV and III-V semiconductors that generally have large refractive indices, high nonlinear susceptibilities as well as a high transparency for frequencies below their electronic bandgap, making them excellent candidates for nonlinear nanoscale applications.[1–3] Similar characteristics appear in 2D materials and more specifically transition metal dichalcogenides, however, their naturally small interaction volume yields only low absolute signal and lowers the damage threshold due to high excitation intensities.[4]

All-dielectric nanoantennas have shown efficient harmonic generation[5–13] and ultrafast nonlinear optical switching[14–17] in various materials such as silicon, (aluminum) gallium arsenide, gallium phosphide (GaP), or germanium. By acting as nanocavities they open the path to larger interaction volumes while maintaining strong resonant behavior with a high tolerance to incident field intensities. Particularly the magnetic dipole[7–9,13] and anapole resonances[5,6]

R. Tirole, S. Vezzoli, R. Sapienza, S. A. Maier
The Blackett Laboratory
Department of Physics
Imperial College London
London SW7 2BW, UK
E-mail: r.sapienza@imperial.ac.uk; stefan.maier@monash.edu

B. Tilmann, L. de S. Menezes
Chair in Hybrid Nanosystems
Nanoinstitut München
Ludwig-Maximilians-Universität München
80539 München, Germany

L. de S. Menezes
Departamento de Física
Universidade Federal de Pernambuco
Recife-PE 50670-901, Brazil

S. A. Maier
School of Physics and Astronomy
Monash University
Clayton Victoria 3800, Australia

The ORCID identification number(s) for the author(s) of this article can be found under https://doi.org/10.1002/adom.202302069

© 2024 The Authors. Advanced Optical Materials published by Wiley-VCH GmbH. This is an open access article under the terms of the Creative Commons Attribution License, which permits use, distribution and reproduction in any medium, provided the original work is properly cited.

DOI: 10.1002/adom.202302069

of nanodiscs have been exploited for harmonic generation given their characteristic strong field confinement within the medium. These single-particle modes can also be used as building blocks for collective resonances: dielectric metasurfaces with various geometries were shown to exhibit high quality factors,[18–21] emerging from bound states in the continuum or constructive interference between single-antenna modes and lattice resonances.

In addition to mode engineering by changing the geometry of nanostructures, an alternative approach is based on the integration of multiple materials in a single antenna.[22–26] In particular, creating a gap inside a high-index dielectric structure in the lateral direction, a slot, filled either with air or a low-index material has the potential to have great impact on the linear and nonlinear properties of the system.[27] Given the optical contrast between dielectric (refractive index n_d) and gap (refractive index n_s), the field intensity scales as n_d^4/n_s^4 from the continuity of the electric displacement field at an interface $n_{d,\,ns}$.[28] Moreover, as long as the slot's dimensions are significantly smaller than that of the the effective wavelength, the far field optical properties of the antenna are retained, as well as its resonant behavior, as determined by the effective refractive index. This makes these nanogap antennas promising candidates for nonlinear nanophotonic applications,[29] however, the experimental realization of different materials in a single nanostructure remains challenging. Only recently, a nanogap using a low index material, indium tin oxide (ITO), slotted in silicon was demonstrated and used for enhanced harmonic generation.[30] ITO shows a zero-crossing of the real part of the dielectric function in the near-IR, allowing for the realization of a nanogap with high optical contrast. It was also shown that ITO exhibits large optical nonlinearities in the vicinity of this so-called epsilon-near-zero (ENZ) regime.[31–33] Hence, the implementation of ITO within other nanophotonic materials of interest could open up new avenues, such as reconfigurable nonlinear generation of light.

In this work, we realize and characterize a nanogap antenna made of high-refractive index GaP and a nanolayer of ITO and compare it to a pure GaP antenna of similar dimensions. We design the nanostructures to exhibit strong optical resonances in the ENZ region, dominated by the magnetic dipole (MD) contribution. Under illumination with near-IR light, we observe comparable second- and third-harmonic generation (SHG, THG) in both antenna designs, whereas the nanogap antenna exceeds the efficiency of the GaP-only case particularly for excitation at the electric dipole (ED) resonance. We show that this enhancement appears over a broad wavelength range, exceeding the ENZ regime of ITO. To explain this result, we perform a thorough analysis of the nonlinear coefficients of both materials and conduct nonlinear scattering simulations. Our results proposes the concept of nanogap antennas as a new and flexible platform with a wide range of possible applications in nonlinear optics. Furthermore, it opens the path of integrating ITO or other ENZ materials into dielectric structures to enhance specific optical resonances of the directivity of emission, as well as time-modulated antennas for frequency control and holography.[34,35]

2. Design and Fabrication

GaP-ITO-GaP films are fabricated by a multi-step sputtering process at elevated temperature, more details can be found in the Supporting Information. The materials were chosen such that a high optical contrast between the two layers is achieved, confirmed by the measured refractive indices shown in **Figure 1a**, while maintaining losses low. The ENZ point of the ITO layer lies around 1300 nm, a regime where GaP shows a high refractive index and virtually no optical losses. Within the ENZ region, ITO exhibits a low refractive index ≈0.4 and acceptable losses at the same level of 0.4, making the material well suited for the realization of a nanogap structure. In a nanodisc with an ITO film located in the center, as sketched in Figure 1b, the contrast of the permittivity at the ENZ wavelength reaches a maximum of more than ten, which leads to a strong confinement of the electric field inside the ITO layer (see Figure 1c). The fabrication of the nanostructures is carried out by electron-beam lithography (EBL) and subsequent reactive ion etching (RIE), more details can be found in the Methods. The distance between individual antennas is kept at 3 µm to prevent cross-antenna coupling. GaP-only nanodiscs with identical dimensions were fabricated following the same process. A scanning electron microscopy (SEM) image of the nanogap discs with varying radii is shown in Figure 1d (left). Looking at the tilted SEM image in the right hand side of Figure 1d, one can clearly observe the three distinct layers that confirms the successful fabrication of the nanogap antennas. The fabrication method is robust as consistent measurements of THG are obtained across many arrays.

We perform finite-difference time-domain (FDTD) simulations to investigate the resonant properties of the fabricated structures. Figure 1e shows the evaluated average field enhancement $|E/E_0|^2$ over the antenna, where E_0 is the incoming electric field amplitude and E the local field amplitude, for GaP-only structures, in dependence of the excitation wavelength and nanodisc radius. Clearly, a set of distinct resonances can be identified. By comparison with a multipole decomposition (see Supporting Information), three main contributions can be identified as indicated in Figure 1e. At larger radii, higher order resonances such as the electric and magnetic quadrupoles dominate the intensity spectrum, whereas smaller radii are dominated by MD and ED (dashed lines). Note that the ED contribution to scattering peaks is broad with components at both higher and lower wavelengths of the MD resonance for a given radius (see Supporting Information), but only the longer-wavelength contribution's to field enhancement and nonlinear optics is clearly identifiable. Further scattering simulations carried out for both GaP and hybrid nanodiscs are shown in Supporting Information and confirm that the far-field response is only marginally affected by the presence of the ITO layer (which makes only 7.5% of the volume of the antenna). However, the continuity of the displacement field vector $\mathbf{D} = \epsilon_0\epsilon_r\mathbf{E}$ requires a change in the electric near-field distribution and consequently strongly confines the electric near-field into the low-index region (pink-shaded area in Figure 1c). This is even more pronounced when comparing the simulated near field distributions of the GaP-only nanodisc in Figure 1f and of the nanogap antenna in Figure 1g, for a wavelength of 1160 nm and an antenna with a radius of 200 nm. For the latter, the field is clearly highly concentrated within the 20 nm thin ITO layer with distribution toward the edges of the disc. Contrarily, the near field of a GaP-only antenna under similar conditions has a field broadly confined over the antenna's volume, with maximum intensity values one order of magnitude smaller.

© 2024 The Authors. Advanced Optical Materials published by Wiley-VCH GmbH

21951071, 2024, 9, Downloaded from https://onlinelibrary.wiley.com/doi/10.1002/adom.202302069 by Test, Wiley Online Library on [04/04/2024]. See the Terms and Conditions (https://onlinelibrary.wiley.com/terms-and-conditions) on Wiley Online Library for rules of use; OA articles are governed by the applicable Creative Commons License

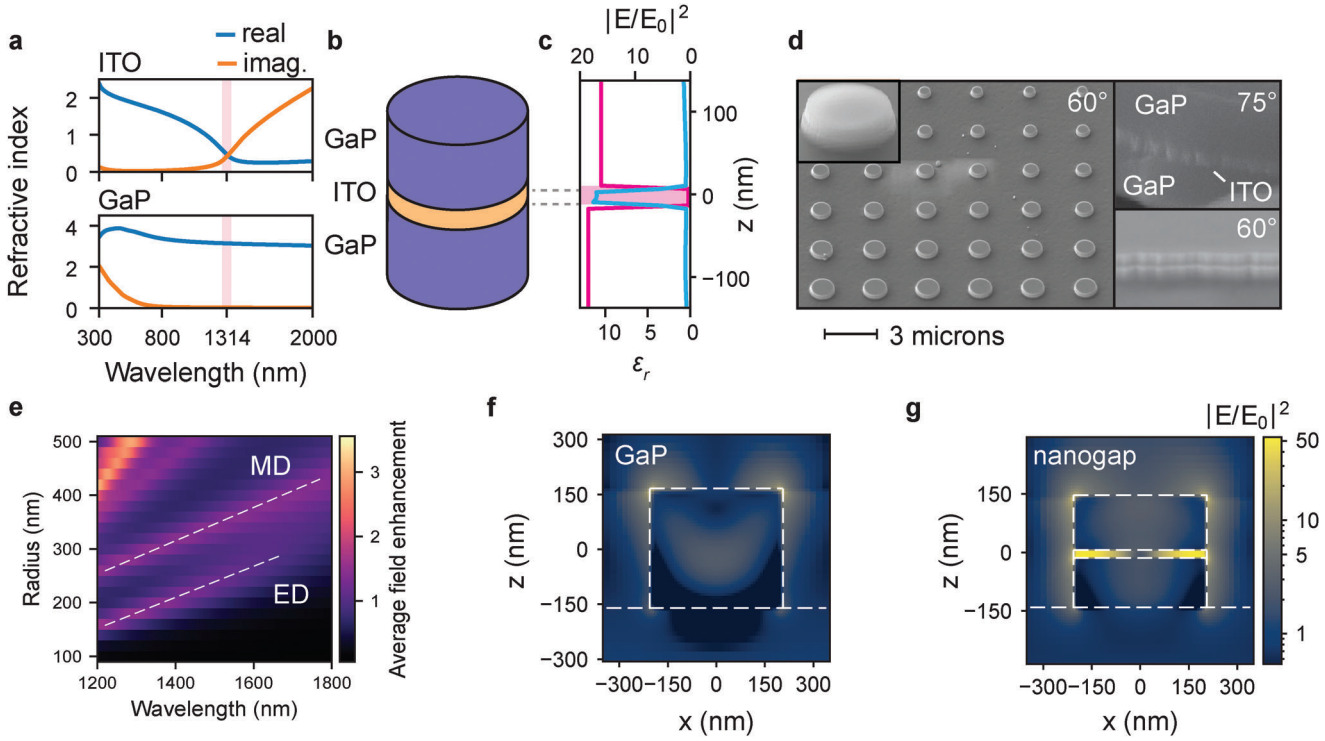

Figure 1. GaP and nanogap antennas for nonlinear frequency generation. a) Refractive index spectra of GaP and ITO, real part and imaginary parts shown in blue and orange, respectively. The ENZ region is highlighted with the red-shaded area. b) Sketch of the nanogap antenna concept. c) Diagram of the expected field intensity distribution (pink) as a function of the centered antenna depth, resulting from the permittivity contrast (light blue). d) Scanning electron microscopy images of the sample, taken at tilt angles of 60 and 75 degrees. e) FDTD simulation of the average field enhancement in a GaP-only antenna as a function of pump wavelength and antenna radius. The ED and MD modes are highlighted with the white dashed curves. f,g) Simulated field intensity profiles in logarithmic scale, in the XZ plane for the GaP (f) and nanogap antennas (g) for a radius of 200 and wavelength of 1160 nm. White dashed lines show the contour of the different materials.

3. Harmonic Generation Measurements

The GaP and nanogap antennas are investigated with respect to their nonlinear optical response by using a nonlinear microscopy setup, based on a tunable wavelength laser with 100 kHz repetition rate and 225 fs (full-width half-maximum) pulses. The generated nonlinear signal is collected in reflection geometry (see **Figure** 2a) and then either sent to a single photon detector or a spectrometer to respectively map the resonances as a function of radius and illuminating wavelength, or measure the light's

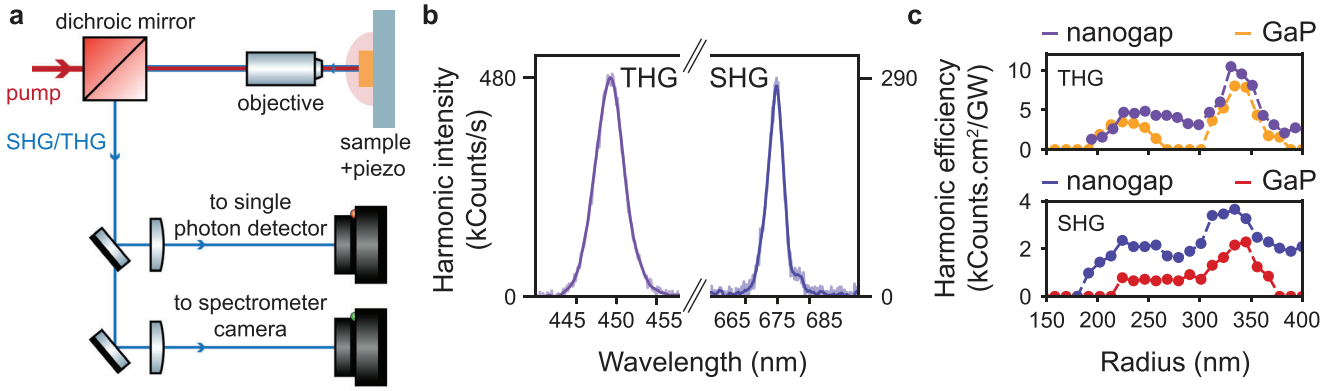

Figure 2. Measurement of harmonic generated light from nanodiscs. a) Experimental microscopy setup for the spectral characterization of antennas. The reflected harmonic from the sample can be sent for detection either by a single photon detector or CCD camera spectrometer. b) Second and third harmonic spectra from a nanogap antenna of 330 nm radius and illumination wavelength of 1350 nm. c) Comparison of THG (top panel) and SHG (bottom panel) efficiency dependence on radius between the nanogap (purple and blue curves) and the GaP-only (yellow and red curves) nanodiscs, for a wavelength of 1350 nm.

© 2024 The Authors. Advanced Optical Materials published by Wiley-VCH GmbH

21951071, 2024, 9, Downloaded from https://onlinelibrary.wiley.com/doi/10.1002/adom.202302069 by Test, Wiley Online Library on [04/04/2024]. See the Terms and Conditions (https://onlinelibrary.wiley.com/terms-and-conditions) on Wiley Online Library for rules of use; OA articles are governed by the applicable Creative Commons License

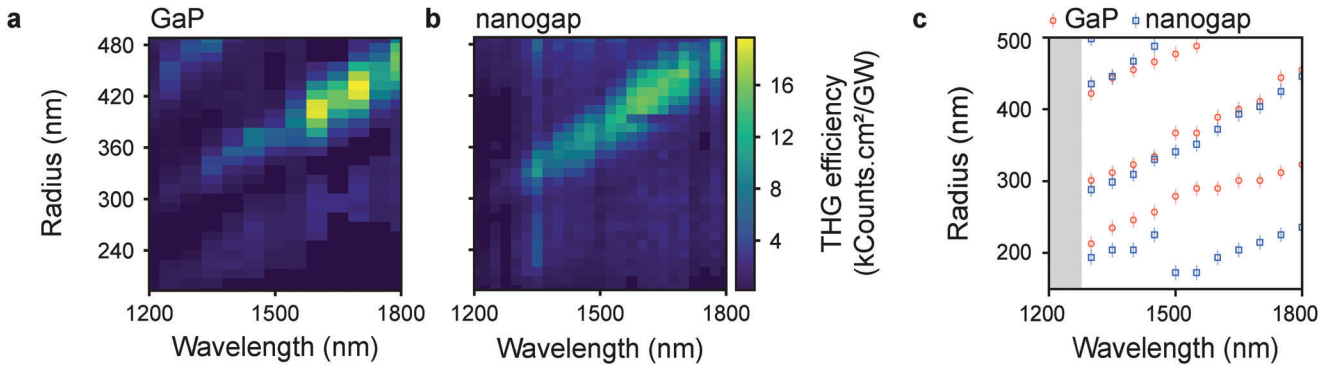

Figure 3. Characterization of the nanodisc's nonlinear signals. a,b) Experimentally measured THG signal in counts per second per unit intensity as a function of disc radius and pump wavelength for GaP (a) and nanogap (b) discs. c) Extracted resonant wavelength for the ED, MD, and EQ modes as a function of radius for the nanogap antenna (blue diamonds), GaP antenna (red diamonds).

spectrum. To calculate the intensity at each wavelength, average excitation power and beam size are measured at the focal position. More details of the experimental setup can be found in the Methods.

For an excitation wavelength of $\lambda_0 = 1350$ nm and a nanogap disc radius of ≈ 330 nm, the corresponding SHG and THG spectra are shown in Figure 2b. The collected light is indeed harmonic centered at $\lambda_{SHG} = 675\,\text{nm} = 1350\,\text{nm}/2$ and $\lambda_{THG} = 450\,\text{nm} = 1350\,\text{nm}/3$, with no evidence for photoluminescence. Furthermore, the nonlinear character of the observed signal is confirmed by power dependence measurements (see Supporting Information). Measurements on a GaP-only disc yield similar results, however, from the amorphous nature of the GaP it is expected that the SHG is largely generated by surface instead of bulk contributions.[36]

Figure 2c shows the SHG and THG signals at a fixed excitation wavelength of 1350 nm in dependence of radius for GaP-only and GaP-ITO antennas. In the case of THG (top panel), the enhancement of the nanogap (purple) against GaP (dark yellow) is limited at the visible ED and MD modes, with only an enhancement by a factor of 1.3 (respective values of 10.45 and 8.01 kHz.cm^2/GW). Yet, the resonances are significantly broadened over a range of radii, with THG counts staying at a constant level between 230 and 300 nm radius. For SHG on the other hand, the nonlinear signal is enhanced over a broad range of radii (blue against red lines, bottom panel). This can be explained by the added amount of interfaces between layers, essential in the generation of the second harmonic as it increases the surface area where SHG occurs,[37] along with a potential higher second order nonlinear susceptibility from the surface of ITO.

Next, we characterize the spectral dependence of the harmonic generation and the evolution of the nanodisc resonances by varying the incident light pulse wavelength. **Figure** 3a shows the measured THG counts per unit intensity for antennas without the ITO layer, in dependence of radius and excitation wavelength. Three distinct resonances are clearly visible, and can be associated to the scattering simulation in Figure 1e. It follows that the lower resonance is caused by the scattering peak that was associated with the ED resonances, whereas the second follows the course of the MD scattering dip. The resonance that is visible at the largest radii can be assigned to the higher order electric quadrupole (EQ). The THG signal that is generated from the MD is more than one order of magnitude larger than for ED. This can be explained by near field simulations (see Supporting Information), where the MD strongly concentrates the electric field inside the volume of the nanostructures. Furthermore, this is confirmed by nonlinear scattering simulations that are shown in the Supporting Information and which qualitatively reproduce the measured THG signal with good agreement.

Following the same procedure, THG was measured for the nanogap antenna, with the spectral and radial dependencies shown in Figure 3b. Again, the previous three resonances can clearly be seen, with the ED, MD, and EQ appearing at similar radii and wavelengths as for the GaP-only structures. One can see the MD mode surprisingly yields less signal further in the IR, around 1650 nm wavelength, but presents comparable if not slightly higher efficiency in the range near its ENZ wavelength (1300–1400 nm). Furthermore, the mode is spectrally broader, and the nanogap antenna exhibits a higher THG efficiency off resonance compared to the GaP-only case. Defining conversion efficiency as $\eta = P_{\text{THG}}/P_{\text{fund}}$, where P_{THG} and P_{fund} are the measured THG and illuminating powers respectively, both the GaP and nanogap antenna exhibit efficiencies of $\approx 10^{-8}$ for the powers used in Figure 3a,b, and a maximum recorded efficiency of 1.97×10^{-7} for an input power of 8.9 μW. This is comparable to values presented in literature for single antennas made of silicon (10^{-7} magnetic resonance)[38] or germanium (10^{-6} anapole mode).[6]

The nanogap antenna shows a distinctive feature in mode evolution when compared to the GaP antenna in its ED resonance. Figure 3c represents the extracted resonant radii of the discs for each excitation wavelength. Each diamond corresponds to a mode's most efficient radius for THG for a given wavelength. All three modes are clearly visible for GaP (light red), and as expected the optimal antenna resonant radius increases with wavelength for each mode as the GaP antenna is a cavity. This is verified by nonlinear scattering simulations (see Supporting Information), which agrees very well with the experimental measurement. For the GaP-ITO antenna, a similar behavior can be observed for the MD and EQ resonances, agreeing well with the course of the GaP-only case and the simulations. For the ED however, a particular dip in the resonant wavelength can be observed for the ED mode, that happens around the ENZ region. Here, the resonant radius drops by ≈ 50 nm when the illuminating pump wavelength is increased by the same amount. This is an interesting behavior

© 2024 The Authors. Advanced Optical Materials published by Wiley-VCH GmbH

21951071, 2024, 9, Downloaded from https://onlinelibrary.wiley.com/doi/10.1002/adom.202302069 by Test, Wiley Online Library on [04/04/2024]. See the Terms and Conditions (https://onlinelibrary.wiley.com/terms-and-conditions) on Wiley Online Library for rules of use; OA articles are governed by the applicable Creative Commons License

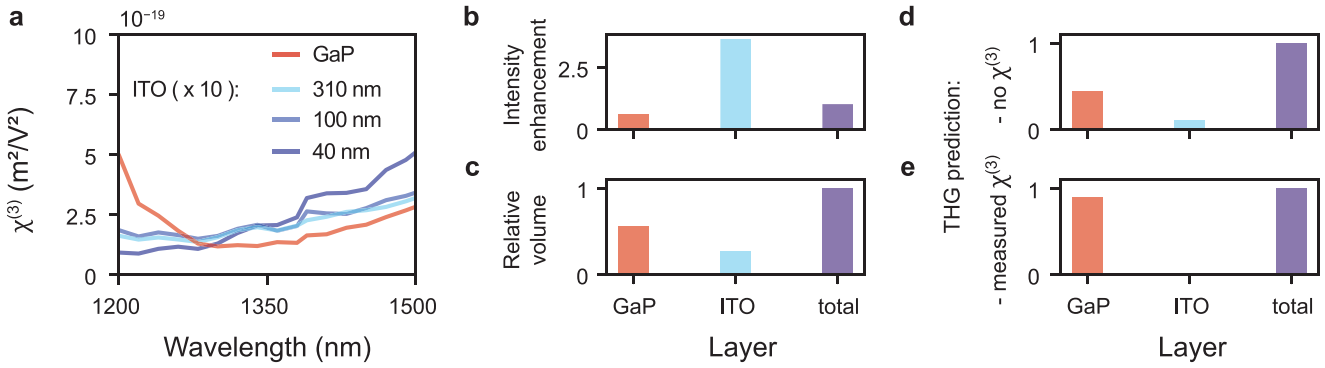

Figure 4. Mechanisms reducing harmonic generation from the ITO layer. a) Measured $\chi^{(3)}$ of various ITO thin films, with 40 nm (dark blue curve), 100 nm (blue curve) and 310 nm (light blue curve) thicknesses, and of GaP (red curve). The nonlinear susceptibilities of ITO are multiplied by ten for comparison. b) Average intensity enhancement with regards to the incoming beam, in the ITO (light blue bar) and GaP (red bar), layers as well as over the entire antenna (purple bar), simulated using FDTD for a 320 nm nanodisc at the MD resonant wavelength of 1520 nm. c) Corresponding intensity enhancement normalized by the volume of the layers or antenna: the comparatively small size of the ITO layer reduces its contribution to the THG signal. d) THG prediction using FDTD, setting $\chi^{(3)}_{GaP} = \chi^{(3)}_{ITO}$: a poor overlap with the harmonic field profile reduces the ITO layer's contribution even further in comparison to the GaP layers. Note that constructive interference between the ITO and GaP layers enhances the harmonic signal. e) THG prediction using FDTD and the experimentally measured nonlinear susceptibility of the materials: the ITO contribution to THG is greatly reduced in comparison to the average intensity enhancement presented in panel b.

that is not predicted by the performed simulations. One possible explanation is that the dielectric constant of ITO is slightly different than the one we have used. In that case, we may miss possible plasmonic resonances with ED character when the ITO becomes metallic. This shift is then caused by the interaction of the antenna's resonance and the plasmonic resonance of the thin ITO layer. The discrepancy in index could originate from the a strong photocarrier excitation occurring due to the field enhancement in the nanogap layer.

4. Nonlinear Susceptibility and Field Distribution

Although an enhancement of the nonlinear signal of a factor up to 2 at resonance from the nanogap compared to the GaP-only antennas could be observed, the effects are not comparable to 100× field enhancement reported in Ref. [30]. To address this discrepancy, we measure and compare the $\chi^{(3)}$ of GaP and ITO in the following. This is done by measuring the samples under weakly focused illumination after which the THG light is collected. Then, the measured harmonic power is processed and compared to the illuminating power to extract a value of the nonlinear susceptibility (see Supporting Information). A 400 nm thick GaP thin film as well as three thin films of ITO with various thicknesses (40, 100, and 310 nm) are investigated. Note that an additional 20 nm ITO thin film was measured, but yielded too weak harmonic signal in the present configuration to give an accurate value for the nonlinear susceptibility. The resulting third order nonlinear susceptibility spectra are presented in **Figure 4a**. As can be seen, GaP (red line) has a $\chi^{(3)}$ an order of magnitude above that of ITO (blue line), with a value of 6.95×10^{-19} m^{2}V^{-2} at 1350 nm wavelength. For comparison, the $\chi^{(3)}$ of silicon is estimated at 3.84×10^{-20} m^{2}V^{-2} at 1650 nm.[39] All three ITO samples, with various thicknesses and different ENZ wavelengths in the near-infrared region, have comparable third order susceptibilities. For this reason, we assume the nonlinear susceptibility of the 21 nm layer of ITO within the nanogap antennas to be equal to that of the 40 nm layer. The reason that the measured $\chi^{(3)}$ is lower than previous reports using Z-scan or pump-probe spectroscopy[32,40] is the following. These techniques are efficient at estimating third order nonlinearities from both photocarrier excitation and the Kerr effect, corresponding to a nonlinear susceptibility tensor of taking the form of $\chi^{(3)}(\omega\,;\,\omega,\,\omega,\,-\omega)$ where the first frequency refers to the outgoing wave and the following ones to the waves interacting via the nonlinearity. For THG, the nonlinear susceptibility is evaluated for different frequencies of $\chi^{(3)}(3\omega\,;\,\omega,\,\omega,\,\omega)$ and can thus take a different value. Thus, observing strong photocarrier excitation nonlinearities in ITO does not guarantee observing efficient THG.

We further investigate the contributions of the ITO and GaP layers within the antenna by looking at FDTD simulations, more precisely at the average field enhancement (normalized to the illuminating field intensity), shown in Figure 4b for a radius of 320 nm, at the MD resonant wavelength of 1520 nm. Clearly, the field is highly concentrated into the ITO layer (light blue box), with a predicted average enhancement of 13.17. From this, the contribution of the ITO layer to the generated THG signal could be approximated to be 13.17^3 larger than that of the GaP layers. But evidently, this did not lead to an increase of the total THG signal in the experiment, which we explain by three contributing factors.

First, the ITO layer occupies only 7.5% of the total nanoantenna's volume. This explains the low shift in the overall antenna resonant radius, but as Figure 4c shows, it also plays against the third harmonic enhancement from the nanogap effect. Multiplying the average field enhancement by the relative volume logically reduces the contribution of the ITO to the total THG by a factor of ten, on a now similar scale to that of GaP.

Second, the antenna's field distribution and resonance at the harmonic wavelength plays an important role in the harmonic generation process.[3,41] In order to enhance the generated signal,

© 2024 The Authors. Advanced Optical Materials published by Wiley-VCH GmbH

21951071, 2024, 9, Downloaded from https://onlinelibrary.wiley.com/doi/10.1002/adom.202302069 by Test, Wiley Online Library on [04/04/2024]. See the Terms and Conditions (https://onlinelibrary.wiley.com/terms-and-conditions) on Wiley Online Library for rules of use; OA articles are governed by the applicable Creative Commons License

the nanodisc needs to provide good overlap between the field distribution and polarization at the fundamental and the harmonic. Nonlinear FDTD simulations (see Supporting Information) in Figure 4d show this is not the case in the ITO layer, which suffers from this constraint in comparison to the GaP layers. The antennas show very little resonance at the third harmonic wavelength due to the high absorption in GaP for energies above the bandgap (around 550 nm). Moreover, the third harmonic is expected to come mostly from the x and y polarised field, orthogonal to the z-polarized field confined in the nanogap layer (see Figure S6, Supporting Information). Nevertheless, constructive interference between the THG signal generated by the ITO and GaP layers can enhance the resulting harmonic signal.

Finally, with the additional effect of the nonlinear susceptibility, the contribution of the ITO layer to the total harmonic generated signal then becomes modest, as shown in Figure 4e.

We have thus shown that the insertion of an ITO nanogap in a high-index dielectric antenna brings little advantage in third harmonic enhancement if the base material shows high nonlinearities. Similar results are expected to hold for AlGaAs, Ge, or $LiNbO_3$, with ITO or AZO as a nanogap layer. Second harmonic generation, on the other hand, is enhanced, which we attribute to the fact it is not generated in the bulk of centrosymmetric materials such as a-GaP or ITO,[37,42] and is proportional to area and not volume, thus mitigating the limited height of ITO. Furthermore, the field distribution is enhanced at the surface of the ITO, while for GaP the field is more evenly distributed throughout the volume.

A potential solution to mitigate the poor fundamental to third harmonic field overlap mentioned previously in the nanogap antenna (see Figure 4d; Figure S6, Supporting Information) would lie in engineering the antenna to support adequate resonances at the harmonic wavelength. In our system, the losses in GaP prevent strong resonances from forming, while ITO becomes dielectric at visible wavelengths, thus damping the nanogap effect and strongly reducing the amount of *z*-polarized light matching the fundamental electric field. By adequately choosing a wavelength range and bulk material to mitigate absorption at the third harmonic, and engineering a double-ENZ cavity[43] to be used as the gap layer, much of the THG nanogap enhancement could be recovered.

Instead, we suggest an alternative application for nonlinear nanogap antennas. To take advantage of the strong Kerr effect and field enhancement within the ITO layer, the nanogap antennas could be used for ultrafast switching and frequency modulation via time-varying effects. By experiencing a strong and swift change in permittivity under pumping at the resonant wavelength, a probe beam at the same wavelength should undergo changes in carrier frequency[44] and spectral width.[45] Then, factors such as overlap and interference of the harmonic field are ruled out, while making use of the strong Kerr nonlinearity of ITO.

5. Conclusion

In summary, we have characterized the crossing between the resonances of a GaP high-index dielectric antenna and the nanogap effect from an ITO thin film, by measuring a broadband enhancement of SHG and THG signals from the nanodiscs. The comparison to a GaP-only antenna shows the conservation of the mode resonances and an increased second harmonic signal across all nanogap antenna radii, while the third harmonic, though slightly enhanced, shows a limited increase in efficiency. We attribute this to a combination of lowered parametric nonlinearities in ITO in comparison to GaP, as well as the limitations of volume and field overlap affecting the overall signal generated by the nanogap layer. Nevertheless, this demonstrates that engineered antennas with ENZ nanolayers can be used for nonlinear light generation with comparable efficiencies than bulk nanodiscs, yet with a broader response and a potential for additional antenna engineering. Further development of these nanodiscs could leverage the exceptional properties of ITO and other transparent conducting oxides for ultrafast switching or time-varying effects.[31,46]

6. Experimental Section

Sample Fabrication: The GaP and ITO films were fabricated by subsequent sputter deposition using an Angstrom deposition tool. During the procedure, the sample holder was kept at a constant temperature of 350 °C, while it was allowed to cool down between the different deposition steps to avoid mixing of the different layers. As substrate, borosilicate cover slips were used and previously cleaned with acetone and isopropyl alcohol (IPA) and ultrasonication. Finally, a 70 nm layer of silicon dioxide was deposited on top of the layer, using plasma enhanced chemical vapor deposition (PECVD, Oxford Instruments). The EBL was preformed using Poly(methyl methacrylate) (PMMA) as photoresist and carried out with a 20 µm aperture, 30 kV acceleration voltage and a dose factor of 400 µCcm^{-2} (e-LiNE, Raith GmbH). After development in methyl isobutyl ketone:IPA (ratio 1:3) for about 50 s and 10 s of oxygen plasma cleaning (20 sccm, 40% power), a 50 nm gold film was deposited on top using electron beam evaporation at ultrahigh vacuum. Next, the lift-off process was performed using Remover 1165 (Microposit) at 80 °C for several hours, removing the remaining PMMA and leaving only the desired structures made of gold. Finally, several steps of inductively- coupled plasma reactive-ion etching (ICP-RIE) were performed to transfer the design into the nanogap material. First, fluorine based chemistry was used to etch into the silicon dioxide layer, while clorine based chemistry removed the nanogap material. In between the two steps, gold etchant (Aldrich) was used to remove the gold.

Numerical Simulation: The FDTD simulations were carried out using the commercial software Lumerical FDTD Solutions (Ansys). The material properties were fitted to the ellipsometric refractive index data shown in Figure 1a. Plane wave illumination and total-field scattered-field source were used to evaluate the optical properties of the nanostructures. Perfectly matched layers were used to avoid reflections at the boundaries of the simulation. FDTD simulations were additionally used as foundation for the calculations in the framework of the nonlinear scattering theory (for more details refer to the Supporting Information). Lastly, the multipole decomposition discussed in the manuscript were based on simulated near fields using FDTD. The actual calculation was carried out using the MENP package for MATLAB[47] and was solved for the dipole and quadrupole contributions of the electric and magnetic fields.

Optical Measurements: 220 fs optical pulses with a 100 kHz repetition rate were generated with a LightConversion Pharos laser, and wavelength was controlled via a LightConversion Orpheus OPA. Light was sent through a 60X objective with NA = 0.85, and collected in reflection. Harmonic signal was separated from the pump beam using a dichroic beam splitter, and SHG was filtered out using a short-pass filter. THG was sent either to a Micro Photon Devices (PDM) single photon detector, or to a Princeton Instruments spectrometer with a Pixis CCD camera. Precise control of the illumination area was achieved with a Piezoconcept C3 3-axis piezo stage.

© 2024 The Authors. Advanced Optical Materials published by Wiley-VCH GmbH

21951071, 2024, 9, Downloaded from https://onlinelibrary.wiley.com/doi/10.1002/adom.202302069 by Test, Wiley Online Library on [04/04/2024]. See the Terms and Conditions (https://onlinelibrary.wiley.com/terms-and-conditions) on Wiley Online Library for rules of use; OA articles are governed by the applicable Creative Commons License

Supporting Information

Supporting Information is available from the Wiley Online Library or from the author.

Acknowledgements

R.T. and B.T. contributed equally to this work. This work was funded by the Deutsche Forschungsgemeinschaft (DFG, German Research Foundation) under Germany's Excellence Strategy, EXC 2089/1-390776260, and the Bavarian programme Solar Energies Go Hybrid (SolTech). The authors also acknowledged the support of the Center of Nanoscience (CeNS). R.S. and S.V. acknowledged funding from the Engineering and Physical Sciences Research Council (EPSRC) (grant no. EP/V048880). S.A.M. additionally acknowledged the Lee-Lucas Chair in Physics and the Centre of Excellence in Future Low-Energy Electronics Technologies, Australian Research Council (CE170100039).

Conflict of Interest

The authors declare no conflict of interest.

Data Availability Statement

The data that support the findings of this study are available from the corresponding author upon reasonable request.

Keywords

harmonic generation, nanogap, optical nanoantennas

Received: August 25, 2023
Revised: January 8, 2024
Published online: February 22, 2024

[1] A. I. Kuznetsov, A. E. Miroshnichenko, M. L. Brongersma, Y. S. Kivshar, B. Luk'yanchuk, *Science* **2016**, *354*, 2472.
[2] A. Krasnok, M. Tymchenko, A. Alú, *Mater. Today* **2018**, *21*, 8.
[3] K. Koshelev, S. Kruk, E. Melik-Gaykazyan, J.-H. Choi, A. Bogdanov, H.-G. Park, Y. Kivshar, *Science* **2020**, *367*, 288.
[4] J. W. You, S. R. Bongu, Q. Bao, N. C. Panoiu, *Nanophotonics* **2019**, *8*, 63.
[5] A. E. Miroshnichenko, A. B. Evlyukhin, Y. F. Yu, R. M. Bakker, A. Chipouline, A. I. Kuznetsov, B. Luk'yanchuk, B. N. Chichkov, Y. S. Kivshar, *Nat. Commun.* **2015**, *6*, 8069.
[6] G. Grinblat, Y. Li, M. P. Nielsen, R. F. Oulton, S. A. Maier, *Nano Lett.* **2016**, *16*, 4635.
[7] B. Tilmann, G. Grinblat, R. Berté, M. Özcan, V. F. Kunzelmann, B. Nickel, I. D. Sharp, E. Cortés, S. A. Maier, Y. Li, *Nanoscale Horiz.* **2020**, *5*, 1500.
[8] J. Cambiasso, G. Grinblat, Y. Li, A. Rakovich, E. Cortés, S. A. Maier, *Nano Lett.* **2017**, *17*, 1219.
[9] L. Carletti, A. Locatelli, O. Stepanenko, G. Leo, C. D. Angelis, *Opt. Express* **2015**, *23*, 26544.
[10] L. Carletti, A. Locatelli, D. Neshev, C. De Angelis, *ACS Photonics* **2016**, *3*, 1500.
[11] R. Sanatinia, S. Anand, M. Swillo, *Nano Lett.* **2014**, *14*, 5376.
[12] R. Camacho-Morales, M. Rahmani, S. Kruk, L. Wang, L. Xu, D. A. Smirnova, A. S. Solntsev, A. Miroshnichenko, H. H. Tan, F. Karouta, S. Naureen, K. Vora, L. Carletti, C. De Angelis, C. Jagadish, Y. S. Kivshar, D. N. Neshev, *Nano Lett.* **2016**, *16*, 7191.
[13] G. Marino, A. S. Solntsev, L. Xu, V. F. Gili, L. Carletti, A. N. Poddubny, M. Rahmani, D. A. Smirnova, H. Chen, A. Lemaître, G. Zhang, A. V. Zayats, C. D. Angelis, G. Leo, A. A. Sukhorukov, D. N. Neshev, *Optica* **2019**, *6*, 1416.
[14] G. Grinblat, M. P. Nielsen, P. Dichtl, Y. Li, R. F. Oulton, S. A. Maier, *Sci. Adv.* **2019**, *5*, 3262.
[15] M. R. Shcherbakov, P. P. Vabishchevich, A. S. Shorokhov, K. E. Chong, D.-Y. Choi, I. Staude, A. E. Miroshnichenko, D. N. Neshev, A. A. Fedyanin, Y. S. Kivshar, *Nano Lett.* **2015**, *15*, 6985.
[16] M. R. Shcherbakov, S. Liu, V. V. Zubyuk, A. Vaskin, P. P. Vabishchevich, G. Keeler, T. Pertsch, T. V. Dolgova, I. Staude, I. Brener, A. A. Fedyanin, *Nat. Comm.* **2017**, *8*, 17.
[17] G. Della Valle, B. Hopkins, L. Ganzer, T. Stoll, M. Rahmani, S. Longhi, Y. S. Kivshar, C. De Angelis, D. N. Neshev, G. Cerullo, *ACS Photonics* **2017**, *4*, 2129.
[18] P. P. Vabishchevich, S. Liu, M. B. Sinclair, G. A. Keeler, G. M. Peake, I. Brener, *ACS Photonics* **2018**, *5*, 1685.
[19] S. Liu, P. P. Vabishchevich, A. Vaskin, J. L. Reno, G. A. Keeler, M. B. Sinclair, I. Staude, I. Brener, *Nat. Comm.* **2018**, *9*, 2507.
[20] S. Campione, S. Liu, L. I. Basilio, L. K. Warne, W. L. Langston, T. S. Luk, J. R. Wendt, J. L. Reno, G. A. Keeler, I. Brener, M. B. Sinclair, *ACS Photonics* **2016**, *3*, 2362.
[21] M. R. Shcherbakov, K. Werner, Z. Fan, N. Talisa, E. Chowdhury, G. Shvets, *Nat. Comm.* **2019**, *10*, 1345.
[22] Y. Zhang, P. Yue, J.-Y. Liu, W. Geng, Y.-T. Bai, S.-D. Liu, *Opt. Express* **2019**, *27*, 16143.
[23] P. Guo, R. D. Schaller, L. E. Ocola, B. T. Diroll, J. B. Ketterson, R. P. H. Chang, *Nat. Comm.* **2016**, *7*, 12892.
[24] H. Aouani, M. Rahmani, M. Navarro-Cía, S. A. Maier, *Nat. Nanotechnol.* **2014**, *9*, 290.
[25] S. Suresh, O. Reshef, M. Z. Alam, J. Upham, M. Karimi, R. W. Boyd, *ACS Photonics* **2021**, *8*, 125.
[26] N. Maccaferri, A. Zilli, T. Isoniemi, L. Ghirardini, M. Iarossi, M. Finazzi, M. Celebrano, F. De Angelis, *ACS Photonics* **2021**, *8*, 512.
[27] Y. Yang, V. A. Zenin, S. I. Bozhevolnyi, *ACS Photonics* **2018**, *5*, 1960.
[28] J. T. Robinson, C. Manolatou, L. Chen, M. Lipson, *Phys. Rev. Lett.* **2005**, *95*, 143901.
[29] A. Patri, K. G. Cognée, D. M. Myers, L. Haeberlé, V. Menon, S. Kéna-Cohen, *Phys. Rev. B Condens. Matter* **2022**, *105*, 165126.
[30] F. Thouin, D. M. Myers, A. Patri, B. Baloukas, L. Martinu, S. Kéna-Cohen, *(Preprint) arXiv:2211.05214, v1, submitted: Nov.* **2022**.
[31] M. Z. Alam, I. De Leon, R. W. Boyd, *Science* **2016**, *352*, 795.
[32] E. G. Carnemolla, L. Caspani, C. DeVault, M. Clerici, S. Vezzoli, V. Bruno, V. M. Shalaev, D. Faccio, A. Boltasseva, M. Ferrera, *Opt. Mater. Express* **2018**, *8*, 3392.
[33] T. S. Luk, D. de Ceglia, S. Liu, G. A. Keeler, R. P. Prasankumar, M. A. Vincenti, M. Scalora, M. B. Sinclair, S. Campione, *Appl. Phys. Lett.* **2015**, *106*, 151103.
[34] N. Karl, P. P. Vabishchevich, M. R. Shcherbakov, S. Liu, M. B. Sinclair, G. Shvets, I. Brener, *Nano Lett.* **2020**, *20*, 7052.
[35] M. Karimi, M. Z. Alam, J. Upham, O. Reshef, R. W. Boyd, *Nanophotonics* **2023**, *12*, 1733.
[36] B. Tilmann, T. Huq, T. Possmayer, J. Dranczewski, B. Nickel, H. Zhang, L. Krivitsky, A. I. Kuznetsov, L. de S. Menezes, S. Vezzoli, R. Sapienza, S. A. Maier, *Adv. Opt. Mater.* **2023**, *11*, 2300269.
[37] Y. R. Shen, *Optical Second Harmonic Generation at Interfaces* **1989**, *40*, 327.
[38] M. R. Shcherbakov, D. N. Neshev, B. Hopkins, A. S. Shorokhov, I. Staude, E. V. Melik-Gaykazyan, M. Decker, A. A. Ezhov, A. E. Miroshnichenko, I. Brener, A. A. Fedyanin, Y. S. Kivshar, *Nano Lett.* **2014**, *14*, 6488.
[39] G. Grinblat, Y. Li, M. P. Nielsen, R. F. Oulton, S. A. Maier, *ACS Nano* **2017**, *11*, 953.

© 2024 The Authors. Advanced Optical Materials published by Wiley-VCH GmbH

21951071, 2024, 9, Downloaded from https://onlinelibrary.wiley.com/doi/10.1002/adom.202302069 by Test, Wiley Online Library on [04/04/2024]. See the Terms and Conditions (https://onlinelibrary.wiley.com/terms-and-conditions) on Wiley Online Library for rules of use; OA articles are governed by the applicable Creative Commons License

[40] M. Z. Alam, S. A. Schulz, J. Upham, I. De Leon, R. W. Boyd, *Nat. Photon.* **2018**, *12*, 79.
[41] K. O'Brien, H. Suchowski, J. Rho, A. Salandrino, B. Kante, X. Yin, X. Zhang, *Nat. Mater.* **2015**, *14*, 379.
[42] R. W. Boyd, *Nonlinear Optics*, Elsevier, Amsterdam **2020**.
[43] V. Caligiuri, M. Palei, M. Imran, L. Manna, R. Krahne, *ACS Photonics* **2018**, *5*, 2287.
[44] K. Pang, M. Z. Alam, Y. Zhou, C. Liu, O. Reshef, K. Manukyan, M. Voegtle, A. Pennathur, C. Tseng, X. Su, H. Song, Z. Zhao, R. Zhang, H. Song, N. Hu, A. Almaiman, J. M. Dawlaty, R. W. Boyd, M. Tur, A. E. Willner, *Nano Lett.* **2021**, *21*, 5907.
[45] R. Tirole, E. Galiffi, J. Dranczewski, T. Attavar, B. Tilmann, Y.-T. Wang, P. A. Huidobro, A. Alú, J. B. Pendry, S. A. Maier, S. Vezzoli, R. Sapienza, *Phys. Rev. Appl.* **2022**, *18*, 054067.
[46] E. Galiffi, R. Tirole, S. Yin, H. Li, S. Vezzoli, P. A. Huidobro, M. G. Silveirinha, R. Sapienza, A. Alú, J. B. Pendry, *Adv. Photonics* **2022**, *4*, 014002.
[47] T. Hinamoto, M. Fujii, *OSA Contin.* **2021**, *4*, 1640.

© 2024 The Authors. Advanced Optical Materials published by Wiley-VCH GmbH

21951071, 2024, 9, Downloaded from https://onlinelibrary.wiley.com/doi/10.1002/adom.202302069 by Test, Wiley Online Library on [04/04/2024]. See the Terms and Conditions (https://onlinelibrary.wiley.com/terms-and-conditions) on Wiley Online Library for rules of use; OA articles are governed by the applicable Creative Commons License